Mössbauer Spectroscopy

MIT Department of Physics
(Dated: November 29, 2012)

The Mössbauer effect and some of its applications in ultra-high resolution gamma-ray spectroscopy are explored. The Zeeman splittings, quadrupole splittings, and chemical shifts of the 14 keV Mössbauer gamma-ray line emitted in the recoilless decay of the first excited state of the ^{57}Fe nucleus are measured in iron and in various iron compounds and alloys. From the data and knowledge of the magnetic moment of the ^{57}Fe ground state one determines the magnetic moment of the first excited state. Strength of the magnetic field at the sites of the iron nuclei in metallic iron, Fe_2O_3, and Fe_3O_4 are determined. The natural line width of the 14 keV transition is determined from measurements of the absorption line profiles in sodium ferrocyanide absorbers of various thicknesses. Relativistic time dilation is demonstrated by a measurement of the temperature coefficient of the energy of the 14 keV absorption lines in enriched iron.

PREPARATORY PROBLEMS

1. Derive an exact relativistic expression for the recoil energy of the nucleus of mass M that emits a gamma ray of energy E, and evaluate it for an iron nucleus and $E = 14.4$ keV.

2. Suppose the above atom is embedded in an iron crystalite which has a mass of $10^{-6}g$ grams and is free to move. Compute the recoil energy of the crystal. If the emission of the gamma ray is "recoilless", i.e. the nucleus does not acquire momentum relative to the center of mass of the crystal, what would be the energy shift of the gamma ray photon due to the recoil of the crystal?

3. Draw an energy level diagram of the $^{57}_{26}$Fe nucleus in a magnetic field and show the transitions which give rise to the Zeeman pattern you expect to see in this experiment.

4. Why is the multiplicity of energy levels of a nucleus due to electric quadrupole interaction with an electric field gradient acting alone (quadrupole splitting) less than the multiplicity of levels due to magnetic dipole interaction with a magnetic field (Zeeman splitting)?

5. How fast must the source be moved relative to the absorber to shift the frequency of resonant absorption by the natural line width?

6. Why can't you do this experiment with the 6.4 keV photons also emitted by the source?

I. INTRODUCTION

The resolution of a spectrum measurement is characterized by the ratio $E/\Delta E$, where E is the energy of the spectrum line and ΔE is a measure of the line width , e.g. the full width at half maximum. The NaI scintillation spectrometer in the Compton experiment produces a spectrum of 662 keV gamma rays with a resolution of about 10. At the same energy the spectrum obtained with the germanium solid state cryogenic detector in the X-ray Physics experiment has a resolution of 200. The high resolution gratings used in the hydrogenic atom experiment for measurements in the visible portion of the spectrum has a resolution on the order of 5×10^4.

Now imagine spectroscopy with a resolution of 10^{12}! "Recoilless" emission and resonance absorption of gamma radiation by nuclei discovered by Rudolf Mössbauer in 1957 makes possible such ultra-high resolution spectroscopy in the gamma-ray region of the spectrum. Mössbauer spectroscopy has been used in many areas of physics and chemistry, for example in the determination of life-times of excited nuclear states, in the measurement of nuclear magnetic moments, in the study of electric and magnetic fields in atoms and crystals, and in the testing of special relativity and the equivalence principle. The phenomenon itself is also of great interest. In this experiment you will observe the Mössbauer effect and explore several of its applications in ultra-high resolution spectroscopy.

Mössbauer himself provided a particularly lucid introduction to the physics and application of recoilless gamma-ray emission and absorption in his 1961 Nobel Lecture which is available in the Junior Lab E-Library [1]. More technical discussions are found in [2, 3]. An excellent reference is "The Mössbauer Effect" by Hans Frauenfelder [4] which contains historical and theoretical background and reprints of articles bearing on all the topics in this set of experiments.

You will use as the source of recoilless gamma rays a commercial Mössbauer source consisting of $^{57}_{27}$Co diffused into a platinum substrate. The $^{57}_{27}$Co nucleus decays by K-electron capture to an excited state of $^{57}_{26}$Fe according to the scheme shown in Figure 1. The newly created iron atom settles down in the crystal lattice of the substrate and the d-shell vacancies in its electronic structure are filled in such a way as to eliminate the magnetic field at the nucleus. 91% of the excited iron nuclei decay by gamma-ray emission to the first excited state (3/2-). The latter has a comparatively long half-life of 9.8×10^{-8} seconds (beware that both Melissinos (2003) and Fraunfelder (1962) list the lifetime incorrectly as 0.14 μs) and decays to the ground state with the emission of 14.4 keV

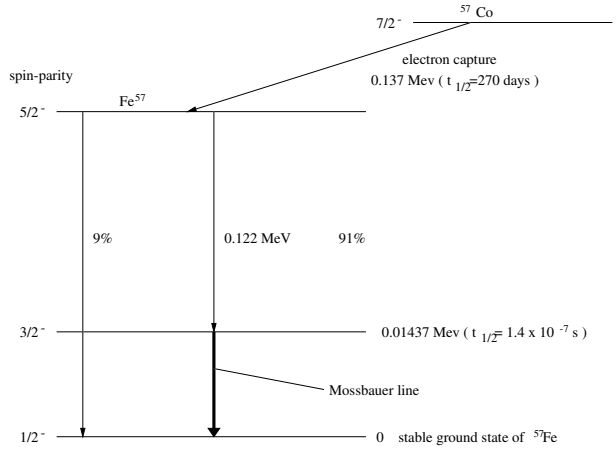

FIG. 1. Decay scheme of $^{57}_{27}$Co. The 14.4-keV transition $3/2- -> 1/2$ is the one used in many Mössbauer experiments. From http://isotopes.lbl.gov/.

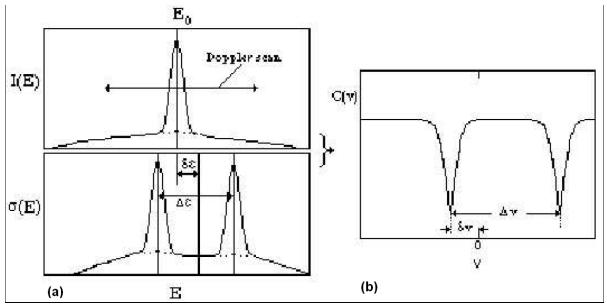

FIG. 2. (a) Schematic plots against energy, E, of (top) the intensity, I(E), of gamma rays from a single line Mössbauer source moving with velocity v relative to a Mössbauer absorber, and (bottom) absorption cross section $\sigma(E)$ of the absorber. (b) Schematic plot of counting rate C(V) of a detector exposed to the gamma rays after they have traversed the absorber against velocity V. In (a) the energy separation of the two absorption lines is $\Delta\epsilon$, and the Doppler shift due to the motion of the source is $\delta\epsilon$. In (b) the velocity separation of the two lines is $\Delta V = c\frac{\Delta\epsilon}{E_0}$, where E_0 is approximately the average energy of the two lines.

gamma rays of which a substantial fraction are emitted without recoil or Doppler broadening. The natural line width of the 14.4 keV line is $\Gamma = \frac{h \ln 2}{2\pi\tau_{1/2}} = 4.7 \times 10^{-9}$ eV corresponding to a fractional width of $\approx 3\times10^{-13}$. In the absence of a field, the magnetic substates of the excited and ground states are degenerate. Under this condition the spectrum of gamma rays from the recoilless emissions appears as a single ultra-narrow line on top of a Doppler-broadened and recoil-shifted "normal" emission line, as illustrated in Figure 2a.

In a similar way, absorbers containing $^{57}_{26}$Fe can have ultra-narrow recoilless resonance absorption lines on top of a normal Doppler-broadened and recoil-shifted 14.4 keV line. Mössbauer absorption lines may be shifted slightly in energy with respect to the emission line by virtue of the different electronic environments of the nuclei in the source and the absorber (the "chemical" shift), and they may be split by the interactions between the nuclear magnetic dipole and/or electric quadrupole moments with internal or external fields in the absorber (Zeeman or electric quadrupole splittings). In a famous experiment that tested the red shift predicted by the general theory of relativity, the shift was caused by a ≈ 100 foot difference in height of the source and absorber!

Figure 2b is a schematic representation of the absorption cross section of $^{57}Fe^{++}$ in an ionic compound in which the iron nuclei are in a nonuniform electric field which produces an electric quadrupole splitting $\Delta\epsilon$ in addition to an isomer shift $\delta\epsilon$ (see below). The measurement process in Mössbauer spectroscopy uses the Doppler shift produced by controlled motion of the source to scan the emission line back and forth in energy over the absorption spectrum of a sample containing the same isotope in its ground state and in a particular chemical or physical environment of interest. The advantage of using a source with a single emission line for performing such a scan is apparent from a consideration of the complications that occur if a multi-line source is used to scan the absorption spectrum of a multi-line absorber.

A primary objective of this experiment is to determine the width of the convolved recoilless emission and absorption lines of the 14.4 keV transition in $^{57}_{26}$Fe. The velocity width Γ_ν corresponding to a given energy width Γ is given by the simple formula $\Gamma_\nu = c\Gamma/E_0$ where E_0 is the mean energy (14.4 keV) of the gamma rays in the line, and c is the speed of light. The velocity width corresponding to the natural line width estimated above is 1×10^{-4} m s^{-1}. Clearly, one will require a velocity resolution at least an order of magnitude smaller to obtain a useful profile of the line shape.

Suppose that the recoilless photons are emitted with a distribution in energy, $I(E)$, centered around E_0. When the source moves at a velocity V toward the absorber, a photon emitted with energy E in the rest frame of the source has an energy

$$E' = E\left(1 + \frac{V}{c}\right) \tag{1}$$

in the rest frame of the absorber. (By convention, positive velocity indicates the source moving toward the absorber.) Call $\sigma(E)$ the cross-section for absorption by the absorber atoms of photons of energy E, and call η the effective area of the detector which we assume to be constant over the narrow energy range of the 14.4 keV line. Then the counting rate when the emitter is moving

with velocity V will be

$$C(V) = \eta \int_0^\infty I(E) e^{-\frac{\sigma(E')Nx}{A}} dE, \tag{2}$$

where x is the thickness of the absorber in g cm^{-2}, A is the atomic weight, and N = 6.022 x 10^{23} mol^{-1} is Avogadro's number. We assume that both the emission line intensity and the absorption cross section have the Lorentzian form, i.e.

$$I(E) = \frac{I_0(\frac{\Gamma}{2})^2}{(E-E_0)^2 + (\frac{\Gamma}{2})^2}, \text{ and} \tag{3}$$

$$\sigma(E) = \frac{\sigma_0(\frac{\Gamma}{2})^2}{(E-E_0-\Delta E)^2 + (\frac{\Gamma}{2})^2}, \tag{4}$$

where ΔE is the intrinsic shift of the resonance energy in the absorber relative to the source due to chemical or other effects, and I_0 and σ_0 are the values at the line centers. The counting rate of a detector placed in the beam of gamma rays after the beam has traversed the absorber is then

$$C(V) = \eta I_0 \int_0^\infty dE \frac{(\frac{\Gamma}{2})^2}{(E-E_0)^2 + (\frac{\Gamma}{2})^2} e^{-\frac{\sigma_0 \frac{\Gamma}{2}^2}{(E[1+\frac{V}{C}]-E_0-\Delta E)^2+(\frac{\Gamma}{2})^2}\frac{Nx}{A}}. \tag{5}$$

For thin absorbers $\frac{\sigma_0 Nx}{A} \ll 1$, and one can obtain an approximate expression for the line profile by expanding the exponential factor in Eqn. 5 and keeping only the first two terms. The integral can then be evaluated by contour integration in the complex plane to obtain

$$C(V) = C_0\Big(1 - \frac{B}{(\frac{E_0 V}{c} - \Delta E)^2 + \Gamma^2}\Big), \tag{6}$$

where C_0 is a constant that depends on the strength of the source and the thickness of the absorber and B is a constant that depends only on the thickness of the source. This function has a minimum at $V = \frac{\Delta E}{E} c$ and a full width at half maximum (FWHM) of $\frac{2c\Gamma}{E_0}$. For thick absorbers one must resort to numerical integration of equation (5). Figure 3 shows the line profiles for various thicknesses of absorber corresponding to values of $\alpha = \frac{\sigma_0 Nx}{A}$ ranging from 0.1 to 10. The width of the absorption line at half amplitude clearly increases with increasing absorber thickness in the range of thickness where nearly all the recoilless emission is absorbed near the line center, i.e. in the range of "line saturation". One can correct for this saturation effect by measuring the line width as a function of absorber thickness and extrapolating to zero thickness. (Note that in an actual observation the non-recoilless emission causes a background counting rate that does not vary with velocity but does decrease with increasing thickness of the absorber.)

Many interesting effects can be observed in absorption spectra; several are discussed below.

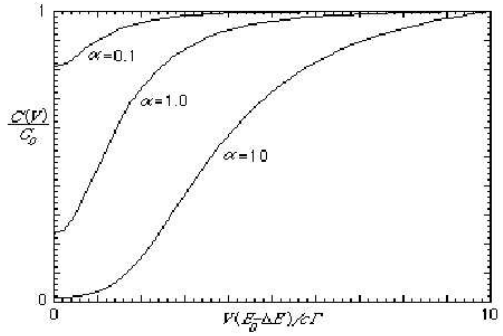

FIG. 3. Calculated shapes of recoilless gamma-ray absorption lines for various thicknesses of absorber. The normalized counting rates are plotted as functions of velocity expressed in units of $\frac{c\Gamma}{E_0 - \Delta E} \approx \frac{c\Gamma}{E_0}$.

II. OBSERVABLE EFFECTS

II.1. Zeeman splitting in an internal magnetic field

The nucleus of an iron atom in metallic iron and certain iron compounds is in an intense magnetic field produced primarily by unpaired electrons of the same atom. Since both the nuclear states involved in the 14.4 keV transition have spin and associated magnetic moments, both are split by the interactions between the nuclear magnetic moment and the magnetic field of the electrons. In an isolated atom the effect of this interaction on optical transitions is characterized as hyperfine splitting. When the atom is bound in a crystal lattice the orientation of the internal magnetic field due to the electrons is fixed with respect to the lattice. As a result, the effect of the electronic magnetic field on the energy of the nucleus may be thought of and analyzed simply as the Zeeman effect in a new context. The number of absorption peaks and their separations depend on the angular momenta and associated magnetic moments of the absorber nucleus in each state. A measurement of the internal Zeeman splitting can be combined with knowledge of the magnetic moment of the ground state (which can be derived from other experiments) to deduce the magnetic field at the iron nucleus in the absorber, and the magnetic moment of the first excited state.

II.2. Isomer shift

If the chemical environment of the iron nuclei in the source and absorber are different then the electron densities will, in general, be different. Since the electromagnetic interaction between the electrons and the nucleus depends, albeit only slightly, on the electron density at the nucleus and on the nuclear radius, and since the radius of the iron nucleus changes slightly in the 14.4 keV transition, there is, in general, a shift of the resonance

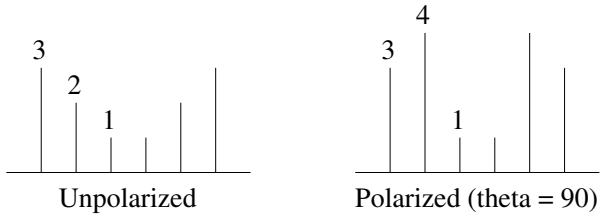

FIG. 4. Expected relative intensities of the Zeeman pattern of ^{57}Fe for an unpolarized absorber and for an absorber polarized perpendicular to the direction of propagation[5].

energy from source to absorber if the host materials are different. This is called the "isomer shift" because the excited states of nuclei were originally called isomers. The magnitude of the shift depends on the s-electron density at the nucleus. If there is greater electron density at the absorbing nucleus than at the emitting nucleus, additional energy must be given to the gamma-ray by moving the source toward the absorber. There are differences on the order of a factor of ten between the isomeric shifts of Fe in the +2 and+3 ionization states in the lattice, and these differences may easily be measured. An isomer shift in a Zeeman or quadrupole pattern appears as a shift of the "center of gravity" of the lines.

II.3. Electric Quadrupole Splitting

The nucleus may be in an electric field with a gradient due to nearby ions with unfilled atomic levels. If the nucleus has a quadrupole (or higher) electric moment, i.e. if its electric charge distribution is not spherically symmetric, its energy levels will be split by amounts that depend on the projections of its spin in the direction of the field gradient. The ground state is shifted by the quadrupole interaction, and the first excited level is split into two levels: thus two transitions with energies $\Delta E_2 \pm \frac{1}{2}\Delta E_3$, are possible, yielding two absorption peaks, as shown in Figure 2.

II.4. Anisotropic emission by polarized nuclei

Each of the possible transitions that give rise to the Zeeman spectrum of lines of an absorber with ^{57}Fe nuclei in a strong internal magnetic field has a particular anisotropic radiation pattern relative to the direction of the field. The orientation of the internal field of a ferromagnetic material can be controlled by a much weaker external field. Thus changes in the relative intensities of the lines in the Zeeman pattern can be caused by placing the absorber in the field of a strong permanent magnet. Figure 4 shows the expected intensities of the Zeeman absorption lines in an absorber with no preferred orientation (unmagnetized) and in an absorber magnetized in a direction perpendicular to the direction of propagation.

II.5. Effect of time dilation on the frequency of the 14.4 keV line

Vibration frequencies of atoms in a crystal at room temperature are of the order of 10^{13} Hertz. Therefore, a ^{57}Fe nucleus in its first excited state makes many oscillations before it decays and, is whizzing around with a mean square velocity of $\approx \frac{kT}{m}$ during this time. According to the special theory of relativity, a clock aboard the moving nucleus runs slow relative to one at rest in the laboratory by the fraction

$$\frac{1}{\gamma} = \sqrt{1 - \frac{v^2}{c^2}}. \tag{7}$$

Thus the center energy of a Mössbauer line emitted from a source at temperature T is shifted down in energy by an amount of the order $\langle(\frac{v}{c})^2\rangle E = \frac{kT}{mc^2}E$, where E is the unshifted energy. The center energy of an absorption line is similarly shifted.

This effect was discovered in the gravitational red-shift experiment by Pound and Rebka (1960). They had to take special care in their experiment to maintain the source and absorber at the same temperature within a fraction of a degree so that the temperature shifts did not mask the gravitational red shift.

The temperature effect provides a clear demonstration of the so-called "twin paradox" of special relativity and resolves any doubt as to whether the accelerations involved in return trips negate the dilation of time suffered by clocks in motion. The exact theory of the effect can be found in the collection of reprints contained in [4].

III. APPARATUS

Figure 5 is a schematic of the experimental arrangement. A beryllium side window proportional gas counter (LND Model 45431, see Melissinos, p 181) and associated measurement chain are used to selectively detect the 14.4 keV photons emitted by excited ^{57}Fe nuclei produced by the beta decay of ^{57}Co in a specially prepared "Mössbauer" source (i.e. ^{57}Co diffused into a platinum substrate). An efficiency curve for the proportional counter is shown in Figure 6. Some of the 14.4 keV photons are emitted by nuclei that share the recoil momentum with macroscopic bits of the matter in which they are imbedded ("recoilless emission") with the result that their fractional spread in energy, or line width, $\frac{\Delta E}{E}$, is extraordinarily narrow, of the order of 10^{-12}.

A sample containing ^{57}Fe atoms in an environment that permits recoilless absorption of 14.4 keV photons, is placed between the source and the proportional counter. The source is mounted on a piston which moves back and forth with a velocity that is a periodic sawtooth function of time. This motion causes a corresponding sawtooth Doppler shift in the energies of the photons that traverse the sample. In effect, the narrow emission line is swept

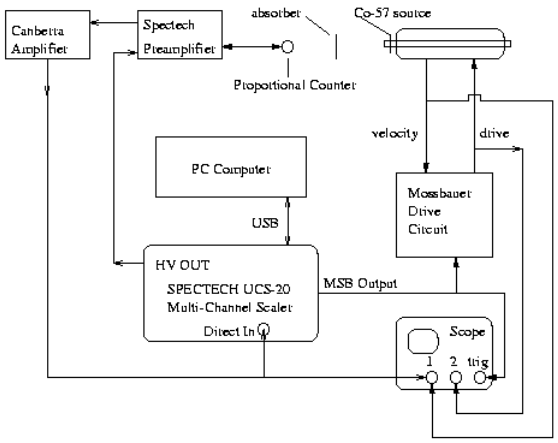

FIG. 5. Block diagram for the Mössbauer spectroscopy experiment. Note that for pulse height analysis measurements of the Co-57 spectrum, the output of the preamplifier should be sent to the 'amp in' input on the back of the UCS20.

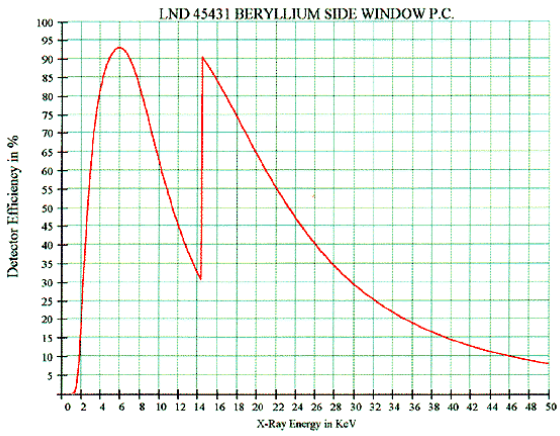

FIG. 6. X-Ray detection efficiency curve for the LND 45431 beryllium side window proportional counter.

back and forth in energy over the recoilless absorption lines of the ^{57}Fe in the absorber. Meanwhile, an external MCA (Spectrum Technologies UCS-20), connected to a PC over a USB bus, operated in its Multi-Channel Scaler or 'MCS' mode, is triggered at the start of each velocity cycle to count clock pulses in a scaler. When a 14.4 keV photon, having traversed the absorber, triggers the proportional counter, the resulting pulse is counted in the memory channel of the MCS with the address given by the current number in the clock scaler. Thus, after a given exposure, each channel of the MCS contains a number of counts proportional to the number of photons that traversed the absorber within the narrow range of energies corresponding to the narrow range of velocities of the piston during which the clock scaler dwelled on the address of that channel.

The detector contains primarily 800 Torr of Krypton with a small amount of methane quench gas. The recommended operating voltage is +1800 VDC with a range of 1700-1950. Typical resolution (%FWHM Cd-109) is 10%. A 14.4 keV photon entering the chamber through the mylar window ionizes some of the Kr atoms, the creation of each ion/electron pair requiring $\geq$ 30 eV. The positive ions drift to the outer wall and the electrons to the center wire. In the viscinity of the wire, E ($\propto 1/r$) is so high that electrons in one mean free path pick up enough energy to ionize more atoms, the effective gas gain being approximately 1000. The methane suppresses the sparking by absorbing the UV quanta generated in the process. Of secondary importance, the methane also supresses the random motion of the electrons, thus shortening the travel time to the center wire and the rise time of the signal pulse. The overall absorption efficiency at 14.4 keV is 30%. The 122 keV and 136 keV photons entering the counter Compton scatter and produce a broad background of lower energy signals. The single channel analyzer (SCA) discriminates against most of these, but about 20% of the pulses falling in the 14.4 keV window of the SCA are from this Compton background. The charge pulse from the counter is amplified and differentiated by the preamp which is mounted as close to the counter as possible. Further amplification of the pulse is provided by the main amplifier.

The contents of each count register are displayed on the computer monitor. In the absence of a Mössbauer absorption line the average number of counts in the various velocity intervals will be equal within the Poisson statistics of counting. If there is a Mössbauer absorption line at an energy equal to the Doppler-shifted energy at some particular velocity, then the counting rate during the time that pulses are addressed to that velocity channel will be reduced, and the accumulated deficiency of counts in that and neighboring channels will be seen as an "absorption line" on the MCS screen.

Detailed instructions for operation of the drive circuit are in a binder located near the equipment. The piston on which the source is mounted is driven by the magnetic force produced by a drive current in the coil of the transducer. The resulting motion induces a current in a sense coil that is proportional to the velocity. This sense current is compared to a reference current ramp, and the difference (error) signal is fed back to the drive-current amplifier in such a manner as to reduce the difference between the sense current and the reference current, keeping the velocity of the piston precisely proportional to the reference current.

The reference current is a sawtooth function of time with a slow, linear rise from $-I_0$ to $+I_0$ with a rapid flyback to $-I$. The corresponding velocity of the piston is therefore also a sawtooth function of time with a slow, linear rise from $-V_0$ to $+V_0$ and a rapid flyback. The MSB signal (most significant bit of the channel address scaler) of the MCS is used to trigger an independent ramp generator in the velocity drive circuit. The circuit is de-

signed for a nominal trigger rate of 6 Hz; it functions satisfactorily at ≈ 5 Hz which is the closest rate that can be obtained from the MCA with the thumb wheels set at [2] and [2]: (200 μs per channel). It is essential that this setting be used. The thumb wheel on the Austin drive adjusts the amplitude of the motion, and hence, with the fixed frequency, the amplitude of the velocity sweep (the rotary switch just below the thumb wheel is not used).

Display both the drive and velocity signals on an oscilloscope and check that 1) the velocity ramp is linear and 2) the drive signal has an average value near zero and is not in high frequency oscillation. The gain in the servo feedback loop, controlled by the FIDELITY knob, should be adjusted to achieve a linear velocity ramp. Start with the knob in the fully Counter-Clockwise position and then cautiously increase until you hear a high pitched tone or until the DRIVE signal begins to oscillate at about 12 kHz. Then, back it off slightly. If you hear a sound emanating from the drive motor, the gain is way too high. The D.C. component should be zero (or nearly so), both on the oscilloscope and as seen on the two LED's just below and on either side of the velocity thumbwheel switch. The COMP. AMP.0 adjustment (on either front panel or on the top of the unit) is used to zero out the D.C. component. At lower velocities, both LED's will be off when adjusted properly. The proper setting of the FIDELITY control is essential to obtaining good and reproducible Mossbauer spectra. There should be a slight ringing after each point in the DRIVE waveform where the sense of the acceleration changes, but this should die out rapidly. The ASYM UL potentiometer control on the top of the unit is used for the flyback generator and should be set for the best straight VELOCITY waveform.

1. **Caution #0: If anything requires adjustment such as changing the thumbwheels to adjust the velocity range, or even if you simply wish to erase the MCS spectrum (clearing the spectrum reinitializes the bistable MSB output) from the software interface, be sure to turn off the MOTOR switch and turn off the software before making the change. Wait about 30 seconds before turning on the motor switch. This allows the unit to stabilize after the bistable has been removed and reapplied.**

2. **Caution #1: The motor switch on the electronic drive generator should be ON only when the MCS is in the 'acquire' mode so the motors are receiving proper ramp voltages.**

3. **Caution #2: Do not touch the fragile window on the proportional counter detector.**

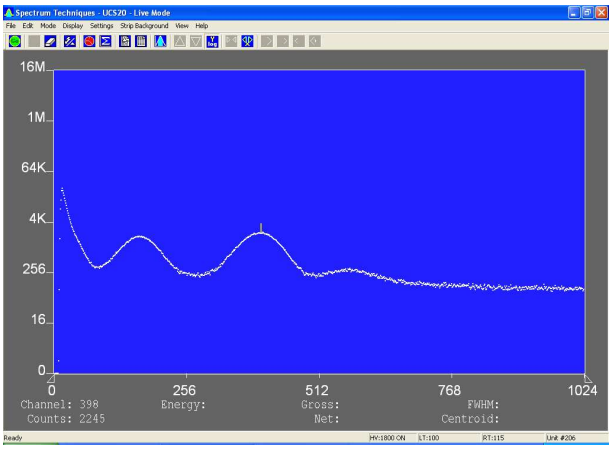

FIG. 7. Typical Co-57 pulse height spectrum acquired by the Spectech UCS-20 multi-channel analyzer. Distance between Co-57 and proportional counter detector window is ∼10cm. Integration time = 100s. Co-57 had ∼5mCi of activity.

III.1. Mössbauer Start-Up Check List

1. Setup the apparatus as shown in Figure 5.

2. Turn on the power switch of the electronics rack and adjust the thumb wheels on the Mössbauer drive to 80. Place the knob marked "Fidelity" in roughtly the central position. (leave the Mössbauer drive switch in OFF position). Turn on the power switch to the SPECTECH UCS-20 Universal Computer Spectrometer.

3. Run the UCS20 Software from the adjacent Windows XP Computer desktop.

4. Use the software menu bar (Settings – Amp/HV/ADC) to turn on the high voltage bias to the propotional counter at +1800 VDC. Also set the conversion gain to 2048.

5. Set the Canberra 816 Amplifier gain to approximately 20.

6. Remove any absorber present in the circular aperture between the Co-57 source and the proportional counter detector. Adjust the carriage holding the source so that it is about 10 cm away from the detector window.

7. Run the MCA in pulse height analysis mode for about 60 seconds and examine the resultant spectrum. It should appear similar to Figure 7. Adjust the gain controls so that the pulses in the strong 6.4 keV iron K-line have an amplitude of about 2.0 volts. Identify the fainter 14.4 keV Mössbauer line at about twice the amplitude of the iron K-line. Hint: a stack of papers roughly the size of this labguide will block the 6.4 keV line but pass the 14.4 keV line.

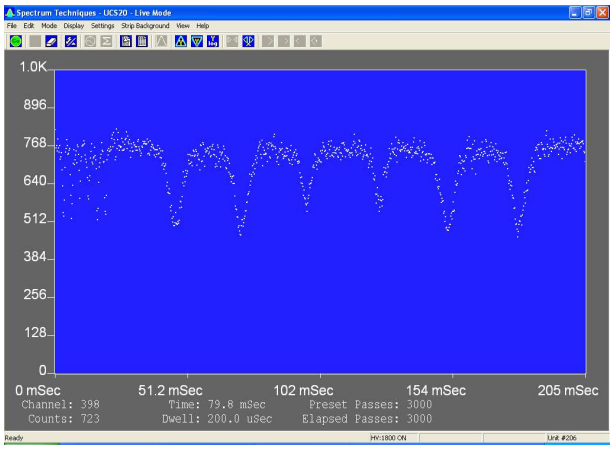

FIG. 8. Typical Mossbauer spectrum using an enriched Fe-57 foil acquired by the Spectech UCS-20 multi-channel analyzer. Distance between Co-57 and proportional counter detector window is ∼10cm. Integration time = 3000 passes ∼10 minutes. Co-57 had ∼5mCi of activity.

8. Adjust the lower and upper level discriminators of the MCA (using the mouse to move the traingles under the 'X' axis) so that only pulses in the 14.4 keV peak are accepted by the ADC (Analog Digital Converter).

9. Place the enriched ^{57}Fe iron foil absorber (**Be Careful!**— found in the white box on the shelf above the apparatus) in the spring clamps between the source and the detector, attempt to center the foil in the circular aperture.

10. Using the software, change the mode from pulse height analysis to Mössbauer. Go to the settings – Mossbauer menu and set the dwell time per channel to 100μs per channel (to give a sweep repetition rate of ≈ 5 Hz). Note that if you change the resolution or "gain conversion" of the software, you must adjust the dwell time per channel to maintain this 5 Hz sweep rate. Set the number of passes to 1500 (5 minutes). Start the MCS acquisition.

11. Turn on the drive and verify that it is moving the piston back and forth at the frequency (≈ 5 Hz) of the MCS sweep. Check the drive and velocity signals using an oscilloscope.

12. Clear the MCS momentarily, start recording, and watch the Mössbauer spectrum of the Zeeman-split 14.4 keV line build up on the MCS screen. After about 5 minutes, you should see something resembling Figure 8.

IV. EXPERIMENTS TO PERFORM

1. Natural width of the 14.4 keV Mössbauer line of ^{57}Fe. The observed linewidths are larger than the intrinsic width of 0.19 mm/s since some broadening is always introduced by inhomogeneity of the environment of the iron in the source and sample. Additional broadening arises from imperfections in the source driving mechanism.

2. Ratio of the magnetic moments of the ^{57}Fe nucleus in its ground and first excited states.

3. Magnetic field at the iron nuclei in metallic iron and in Fe_2O_3.

4. Quadrupole splitting of the first excited state of the ^{57}Fe nucleus in the bivalent and trivalent state of the iron atom.

5. Relative isomer shifts of the 14.4 keV line in metallic iron, steel and compounds of iron.

6. Effect of relativistic time dilatation (second-order Doppler shift) on the frequency of the 14.4 keV line through measurement of the temperature coefficient.

IV.1. Preliminary Experimental Calculations

We now consider the time required to record a Mössbauer spectrum. A typical sample will have 1 mg cm^{-1} of iron in the gamma-ray beam. For purposes of illustration, we assume the spectrum has two absorption peaks. If the Fe57 is present in its natural 2% abundance, there will be 2×10^{17} Fe57 nuclei cm^{-2}. The peak resonant cross section is approximately 2×10^{-18} cm^2 (Frauenfelder, 1963). We divide this value by 8 because of the finite source linewidth, the two absorption peaks of the spectrum, and the estimated product of the recoil free fraction of the source and absorber. The observed intensity will be 5%. The spectrometer will typically divide the velocity scale into 256 channels. For a 10 mCi source the total counting rate is usually about 10,000 counts/s of which about 85% will be 14.4 keV radiation. The spectrometer duty cycle is about 66% and r, the 14.4 keV counting rate per channel, is typically 44 counts/s/channel (you should measure this for yourself!). The signal-to-noise ratio, S/N, is given by $S/N = a_p\sqrt{rT}$where a_p is the peak absorption intensity and T is the running time. If we want a S/N of 40, then for $a_p = 0.05$, T = 14,500s or about 4 hours. For a given S/N, the run time is inversely proportional to the square of the peak absorption.

IV.2. Zeeman splitting of the ground and first excited states of ^{57}Fe in an iron foil

The primary purpose of this part of the experiment is to record and understand the Zeeman splitting of the 14.4 keV gamma-ray line emitted by ^{57}Fe nuclei in an

iron foil. The other purpose is to establish a convenient secondary calibration standard.

Record the absorption spectrum for a sufficient time to obtain at least several thousand counts per channel so that you can measure accurate centroid values, intensities, and shapes of the six lines of the pattern. Measure the channel positions of each of the absorption peaks in the MCS display.

Next, without changing any of the settings, carry out an absolute calibration of the drive motion with the interferometer, as described below. Derive from your measured spectrum and the velocity calibration data the separation in velocity (mm/s) between adjacent pairs of lines in the six-line Zeeman pattern. With these results in hand you can use the quickly observable Zeeman pattern of the enriched iron foil as a secondary calibration standard for each of your subsequent Mössbauer spectrum measurements.

Convert the velocity separations between the lines of the Zeeman pattern into energy separations. The magnetic moment of the ground state of ^{57}Fe has been measured by electron spin resonance techniques to be 0.0903 $\pm$ 0.0007 μ_N. Using this fact, and interpreting the Zeeman pattern in terms of the energy level diagram (see Melissinos, p. 277), determine the internal magnetic field at a nucleus of iron in the iron foil absorber, and the magnetic moment of the first excited state. Discuss the experimental errors in the values you have obtained. With the data in hand can you verify the discovery of Hanna et al. (1960) [5] that the magnetic moments of the ground and first excited states have opposite signs?

IV.3. Absolute calibration

Calibration of the velocity sweep is accomplished with the aid of a Michelson interferometer shown schematically in Fig. 9. A beam of coherent light from a laser is split by partial reflection from a glass slide oriented at 45° so that the two parts traverse different paths before striking the same spot on a photodiode. While the length of one path is fixed, the length of the other path varies because it includes a reflection from a mirror mounted on the moving piston. When the piston moves a distance equal to one-half of the wavelength of the laser light, the length of the path increases by one wave length, the phase of the beam at the photodiode changes by 360°, and the intensity of the recombined beam at the photodiode goes through one cycle of constructive and destructive interference. Every cycle of interference produces one cycle of a sinusoidal voltage signal from the photodiode that can be registered as one pulse by the multichannel scaler. Call V_i the average velocity of the moving mirror during the time interval corresponding to the ith channel of the multichannel scaler display. The average rate of pulses during the ith time interval is $\frac{2V_i}{\lambda}$. If we call T the time interval during which pulses are directed to a given channel by the clock register, i.e., the dwell time per channel,

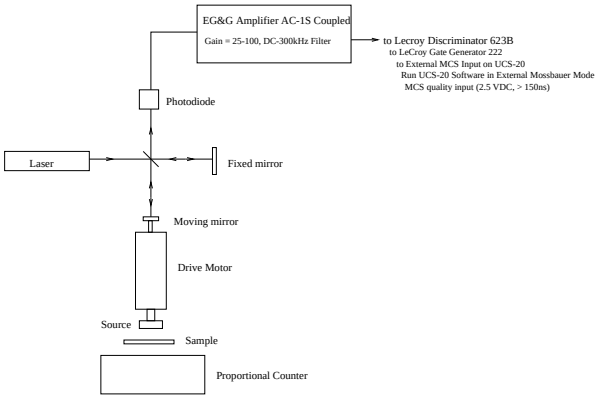

FIG. 9. Schematic diagram of the Michelson interferometer for calibration of the velocity sweep. **Be particularly sensitive to try and block any stray reflections of the HeNe laser from interferometer into another another portion of the lab. Block as necessary using black posterboard or index cards.**

and N the number of sweeps made during the course of a calibration run, then the total number of counts recorded in the ith channel will be:

$$C = NT\Big(\frac{2V_i}{\lambda}\Big). \tag{8}$$

Solving for the velocity corresponding to the ith channel, we find:

$$V_i = \frac{C\lambda}{2NT}. \tag{9}$$

The orientations of the laser, the beam splitter (glass slide), and the two adjustable mirrors should be adjusted so that the incident and reflected beams all strike the beam splitter as close to the same spot as possible without allowing a reflected beam to go straight back into the laser where it may disrupt the performance of the laser. **Be sure to prevent unwanted laser light from crossing the room potentially harming another investigator.** Adjust the mirrors to superpose the two beams of the interferometer on the photodiode.

Operate the UCS20 in 'External Mössbauer' mode and turn on the Mössbauer drive motor. Watch the oscilloscope for the interference signal as you make small adjustments of the mirrors. When you see some interference fringes on the photodiode output, send the signal to the EG&G 5113 Amplifier with a gain of about 10-100 and AC couple the A-input. Apply a low-pass filter with a cutoff of about 300 kHz. This signal is then sent to the LeCroy 623B discriminator converting the analog interference signal into a fast rise time logic level pulse. In order to generate an "MCS-friendly" input, we process the output of the discriminator with the LeCroy 222 Gate Generator. Set the pulse width to 10 microseconds and send the TTL output into the External MCS input on the back of the Spectrum Techniques UCS-20

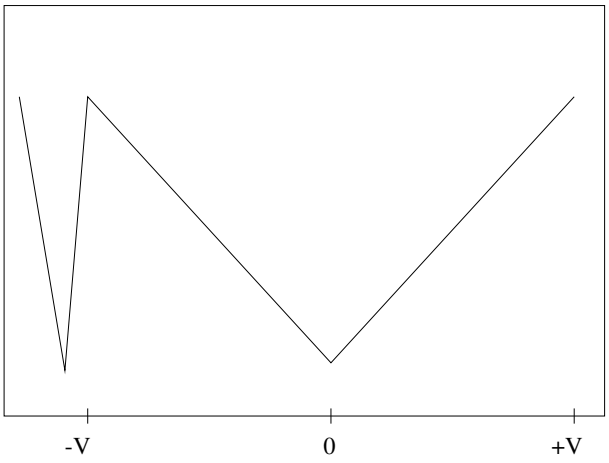

FIG. 10. Ideal appearance of the multichannel scaler screen after several minutes of operation with the interferometer velocity calibrator. The sharp feature at the start is produced during the rapid reversal of the velocity of the piston at the high speed end of its stroke. In reality, the bottom of the "V" will probably be truncated due to the low amplitude of the pulses during the low-velocity portion of the sweep.

instrument. When everything is working properly, the multichannel scaler look similar to Fig. 10.

When you have mastered the calibration procedure, run the Mössbauer setup with an enriched iron foil absorber and adjust the amplitude of the velocity sweep to obtain the 6-line Zeeman pattern that will be your secondary calibrator. Record the channel numbers of the absorption line centroids. Without changing any of the settings of the Mössbauer drive circuit except to turn it off and on, proceed with the interferometer calibration by replacing the proportional counter pulses with the interferometer pulses. If everything is working properly, the velocity sweep should be precisely linear so that $V_i = ai + b$ where 'a' and 'b' are constants. Thus two measurements of the velocity in good (smooth) portions of the calibration "V" pattern are sufficient to determine 'a' and 'b'. Since realigning the interferometer each time a velocity change is made, subsequent velocity calibrations may be made using the known splittings of either metallic iron or Fe_2O_3. Please see the 'ASA-700 Mossbauer Drive' document under the 'Selected Resources' section of the Junior Lab web site for these data.

The following is a menu of possible investigations:

1. Properties of the Resonant Line Shape. In this experiment, you will use an absorber of sodium ferrocyanide $Na_3Fe(CN)_6 \cdot 10H_2O$ which has no magnetic field or electric field gradient at the crystal sites of the iron nuclei. Absorbers of three different thicknesses are available. This allows you to measure the line width as a function of thickness so that you can extrapolate your results to zero thickness. Derive a value for the intrinsic width of the 14.4 keV first excited state of ^{57}Fe and compute the implied lifetime of the excited state. What other causes of line broadening may be present in your data?

2. Temperature coefficient of the Mössbauer lines and the twin "paradox". The temperature effect is a shift in the resonant frequency of an absorption line due to the second order Doppler effect which amounts to a slowing of the atomic "clocks" in a heated sample due to their thermal motion relative to the reference atomic clocks in the lab. According to the theory of relativity, the effect should be of the order of $(\frac{v}{c})^2 \approx \frac{kT}{mc^2} \approx 10^{-13}$. That is small indeed, but accessible to Mössbauer spectroscopy. It is also a proof that the so-called "twin paradox" (not really a paradox since it follows logically from the theory of relativity) is really true, i.e. that if you send your twin on a fast round trip rocket flight he/she will return younger than you. See Reference [4], page 63 for more details. The strategy of this experiment is as follows:

   (a) Operate the spectrometer at very high dispersion and calibrate it by measuring the separation between the two central peaks of the ^{57}Fe spectrum;

   (b) Measure the fractional shift position $\frac{\Delta E}{E}$ of the single peak of stainless steel between room temperature T and $T + \Delta T$;

   (c) Compare the result with the theory of Josephson (page 252 within the Frauenfelder collection).

   To measure the temperature effect reduce the velocity amplitude of the Mössbauer drive so that the two central components of the Zeeman pattern are widely separated, say by 400 channels, i.e. increase the dispersion of the spectrometer so that the small effect of temperature will be able to cause a shift of several channels in the centroids of the Zeeman lines. Calibrate the velocity scale by recording the locations of the central two peaks of the ^{57}Fe spectrum. Place the aluminum-block oven with the Mylar windows, containing the thin stainless steel and attached heater and thermocouple, in position between source and counter. Accumulate a spectrum with sufficient counts so that the positions of the peaks of the absorption line can be determined with an uncertainty no greater than 11 channel.. Adjust the temperature control to $120°C$ and turn on the heater. When the temperature has stabilized record a high-temperature spectrum. Repeat cold and hot measurements several times to reduce and evaluate your random error. Determine the temperature coefficient from your data, i.e. the fractional change in the peak energies per degree centigrade, and compare your results with the theoretical prediction (see the discussion in Frauenfelder, 1962, page 63).

3. Quadrupole splitting and isomer shifts in Fe^{++} and Fe^{+++} ions. Measure the absorption spectra in samples of $FeSO_4 \cdot 7H_2O$ and $Fe_2(SO_4)_3$ and determine the quadrupole splittings (if any) and the isomer shifts. Accumulations of 30 to 60 minutes should be sufficient to show the absorption spectra and permit accurate measurement of the splittings. See [6] for a discussion of the implications of such measurements.

4. Combined Zeeman and quadrupole effects in Fe_2O_3. Measure the absorption spectrum of an isotope-enriched sample of red (ferrous) iron oxide, Fe_2O_3. (Note that the red oxide, otherwise known as rust, is not ferromagnetic, i.e. it is not attracted by a magnet.) Allowing for the combined effects of Zeeman and quadrupole splitting, and using the value for the magnetic moment of the first excited state obtained above, derive the strength of the magnetic field at the iron nuclei in red oxide, and the magnitude of the product of the quadrupole moment and the electric field gradient.

5. The absorption spectrum of magnetite (Fe_3O_4; the black magnetic oxide of iron). Try to figure out what is going on. The available samples of magnetite require long exposures because they have only the natural abundance of 2%. The Mössbauer spectrum of magnetite has provided important clues to the structure of this peculiarly complex substance. You will probably need to dig into the literature for help in the interpretation of the spectrum. There is an extensive series of reviews on Mössbauer spectroscopy in the Science Library. Incidentally, the black sand that you may have seen on ocean beaches is magnetite.

6. Other iron-bearing materials, like rust, cast iron filings, spring steel, medicinal iron pills, black sand.

Other references related to this experiment are [7–12]

[1] *Nobel Lectures from Robert Hofstadter and Rudolph Ludwig Mössbauer*.

[2] A. C. Melissinos, *Experiments in Modern Physics* (Academic Press: Orlando, 2003) ISBN QC33.M523, physics Department Reading Room.

[3] S. Gasiorowicz, *Quantum Physics*, 2nd ed. (Wiley: New York, 1996) ISBN QC174.12.G37, physics Department Reading Room.

[4] H. Frauenfelder, *The Mössbauer Effect* (Benjamin: New York, 1962) ISBN QC477.F845, physics Department Reading Room.

[5] S. S. Hanna, J. Heberle, C. Littlejohn, G. J. Perlow, R. S. Preston, and D. H. Vincent, Phys. Rev. Letters **4**, 177 (1960).

[6] S. DeBenedetti, Sci. Amer.(1960).

[7] Boyle and Hall, Reports on Progress in Physics, XXV **Aug**, 442 (1962), qC.R425, Science Library Journal Collection, London.

[8] O. C. Kistner and A. N. Sunyar, Phys. Rev. Letters **4**, 412 (1960).

[9] O. C. Kistner, A. N. Sunyar, and D. H. Vincent, American Institute of Physics: New York(1963).

[10] S. L. Ruby, L. M. Epstein, and K. H. Sun, Rev. Sci. Instr. **31**, 580 (1960), qC.R453, Physics Department Reading Room.

[11] E. Oldfield and R. Kirkpatrick, Science **227**, 1537 (1985).

[12] U. Gonser, *Mössbauer Spectroscopy*, Topics in Applied Physics, Vol. 5 (Springer-Verlag, 1975) ISBN QC491.M6, pp 16-17.

Model	Description	Source
ASA S-700A	Mössbauer Drive	NA
ASA K-4	Mössbauer Motor	NA
ASA PC-200	Scintillator	no longer available
Canberra 3002D	HV Power Supply	canberra.com
Canberra 815	Amplifier	canberra.com
MG 05-LHR-111	Laser	mellesgriot.com
Ortec 109PC	Pre-Amp.	ortec-online.com
MIT	Low Freq Amp	homemade
MIT	Interferometer Setup	homemade
MIT	St. Steel Absorber/Oven	homemade
MIT	Mössbauer Absorbers	webres.com

Appendix A: Mösssbuaer Effect Equipment List

Appendix B: Verification of Velocity Calibration

To first order, T, the dwell time per channel is simply that which was set under the Mossbauer settings submenu in the UCS-20 software.

This can be confirmed, if desired by feeding pulses from a pulse generator to both the input of the pulse amplifier and to a frequency meter. Integrate for sufficient time to obtain a smooth horizontal pattern and count the number of sweeps. From the number of sweeps, the average number of pulses recorded per channel, and the frequency of the pulses, you can compute T, the dwell time per channel.

Example: Suppose you record N=1000 sweeps and find C=2000 counts in a particular channel. With the ASA-

700 thumb-wheel sweep controls set at 80 mm s^{-1}, you may have found in the frequency-generator calibration that T=170μs ch^{-1}. The wavelength of the HeNe laser light is $\lambda = 6328\mathring{A}$, or 6.328×10^{-5}cm. According to Equation 9, the piston velocity at that part of the cycle is

$$V = \frac{6.328 \times 10^{-5} \times 2000}{1000 \times 0.000170 \times 2} = 0.367\ cm\ s^{-1} \qquad \text{(B1)}$$

Table 1.2. Mössbauer parameters and effects

Symbol	Definition and units used	Corresponds in wave or particle picture, respectively	Physical parameter	Cause of the effects	Observed or predicted effects	Formulation	Fe^{57} energy level diagram with allowed transitions: Source (S) / Absorber (A)	Schematic representation of observation (resonance absorption vs. velocity)
f	Number of recoil free γ-ray events (emission or absorption) divided by total number of γ-ray events, dimensionless (Debye-Waller factor)	Relative intensity of resonance line Probability of recoil-free events	Probability of phonon creation or annihilation by the emitting or absorbing atom or mean square of vibrational amplitude		Intensity of Mössbauer line	$f = \exp - k^2 \langle x^2 \rangle$	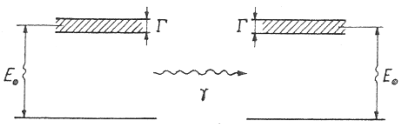	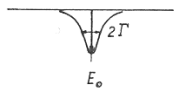
				Vibrational modes of the resonating atom (as function of direction, temperature and pressure, in different lattices, phases, near critical temperatures, at surfaces and close to other lattice defects)	Intensity dependence			
				Vibrational modes of the resonating atom in non-cubic symmetry of single crystals, and polycrystalline materials	Change in the relative line intensities of hyperfine split spectra (Goldanskii-Karyagin effect)			
Γ	Full width at half maximum in energy units	Line width or spread in wave length Uncertainty or spread in energy	Mean lifetime of the excited state Apparent mean lifetime of the excited state Atomic, magnetic electric relaxation processes		Natural line width	$\Gamma_{\text{eff}} = \frac{\hbar}{\tau_{\text{eff}}}$	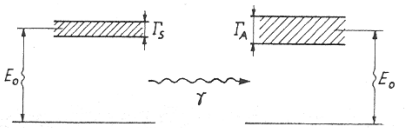	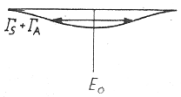
				Saturation effects Diffusion and Brownian motion of the atoms or molecules, Relaxation processes, Spin-flip processes, Superparamagnetism, Fluctuations near critical temperatures (magnetic, ferroelectric and other phase transitions)	Line broadening			
				Delay coincidence measurements Thermal spike	Line narrowing			
				Change in the mean lifetime of the excited state	Line narrowing or line broadening			
E_γ	Mean energy of radiation in energy units	Mean wavelength of γ-radiation Mean energy of γ-radiation	Energy difference between excited and ground state	Interaction of the nuclear charge distribution with the electron density at the nuclei in source and absorber (electric monopole interaction)	Isomer shift	$\delta = C \frac{\delta R}{R} [\lvert\psi_A(0)\rvert^2 - \lvert\psi_S(0)\rvert^2]$	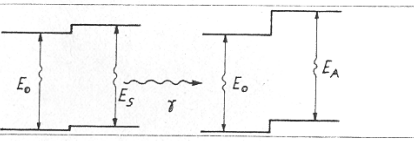	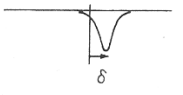
				Interaction of the nuclear magnetic dipole moment with a magnetic field at the nucleus (magnetic dipole interaction); Angular dependence of the nuclear Zeeman effect in single crystals, preferred oriented materials (texture) and polycrystalline materials; Symmetry tests in γ-decay (time reversal invariance, parity conservation); Boltzmann population of the hyperfine sublevels at low temperature ($\ll 1$ K)	Nuclear Zeeman effect Change in the relative line intensities, polarization of the γ-radiation (linear, elliptical, circular) Change in relative line intensities Change in relative line intensities	$E_m = -g_N \beta_N H m_I$	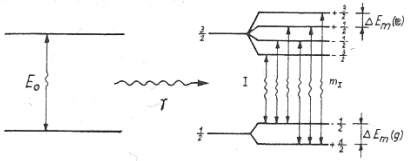	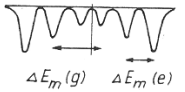
				Interaction of the nuclear quadrupole moment with EFG at the nucleus (electric quadrupole interaction) Angular dependence of the quadrupole interaction in single crystals, preferrentially oriented materials (texture) and polycrystalline materials	Quadrupole splitting Change in the relative line intensities, polarization of the γ-radiation	$E_Q = \pm \frac{1}{4} eQV_{zz} (1 + \frac{1}{3}\eta^2)^{\frac{1}{2}}$	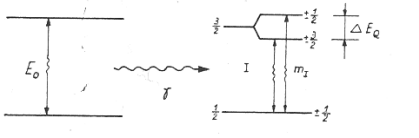	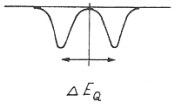
				Change in temperature Change in pressure Acceleration and gravitational fields	Relativistic effects Temperature shift Pressure shift Acceleration and gravitational red shift	$\delta_R = \frac{v^2}{2c^2} E_\gamma$	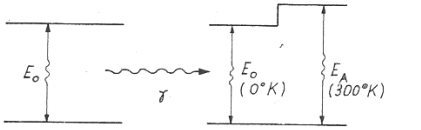	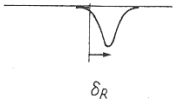

FIG. 11. From Mössbauer Spectroscopy, Edited by U. Gonser, Springer-Verlag, 1975